The Hurst coefficient and lacunarity applied to atmospheric sub-micron particle data

Rubén Darío Arizabalo[*], Eugenio González-Avalos, Gustavo Sosa Iglesias
Instituto Mexicano del Petróleo, Eje Central 152, CP07730, México, D. F.

E-mail: rarizaba@imp.mx

(Received 9 December 2010, accepted 29 June 2011)

Abstract

The study of air pollution is based on the characterization of sub-micrometric atmospheric particles, and the fractal analysis is a new tool for describing them. In order to obtain experimental data about the atmospheric particles emitted by vehicles, a Refinery and a Power Plant in the Tula region (Hidalgo State, Mexico), atmospheric particle concentrations were measured from March 24 to April 24 as part of the MILAGRO campaign (2006) at the Jasso Station by means of an SMPS. From the campaign days, 16 were selected to perform the fractal analysis of the experimental data through the Hurst coefficient (H) and lacunarity (L). In this work, the Hurst coefficient was associated with the variations (roughness) concerning both the particle concentrations and particle formation processes (nucleation, Aitken, accumulation), which are connected with the intensity of the emissions throughout time. As for lacunarity, it provided information about the distribution of the particle sizes (lagoons) and the type of particle formation processes occurring through the sampling days.

Keywords: Atmospheric particles, Hurst coefficient, Lacunarity.

Resumen

El estudio de la contaminación del aire se basa en la caracterización de partículas sub-micrométricas y el análisis fractal es una nueva herramienta para describirlas. Para obtener datos experimentales sobre las partículas atmosféricas emitidas por vehículos, de una refinería y de una Planta de Electricidad en la Región de Tula (Estado de Hidalgo, México) se midieron concentraciones de partículas atmosféricas desde el 24 de marzo al 24 de abril como parte de la Campaña MILAGRO (2006) en la estación de Jasso por medio de un SMPS. De los días de la Campaña, 16 fueron seleccionados para llevar a cabo el análisis fractal de los datos experimentales a través del coeficiente de Hurst (H) y de Lagunaridad (L). En este trabajo, el coeficiente de Hurst fue asociado con las variaciones (rugosidad) observadas en las concentraciones de partículas y en los procesos de formación de partículas (nucleación, Aitken, acumulación), los cuales están asociadas con la intensidad de las emisiones a través del tiempo. Con respecto a la lagunaridad, ésta proporcionó información sobre la distribución de los tamaños de partículas (lagunas) y el tipo de procesos de formación de partículas que ocurrieron a lo largo de los días de muestreo.

Palabras clave: Partículas atmosféricas, Coeficiente de Hurst, Lagunaridad.

PACS: 92.60.Sz, 05.45.Df **ISSN 1870-9095**

I. INTRODUCTION

The study of the multi-scale problem of atmospheric particles is based on the underlying growing mechanisms of sub-micron particles. These complex mechanisms depend on several variables such as particle chemical composition, gas phase concentration and meteorological variables, among others. Accordingly, the use of the fractal theory has been explored as a potential tool to study aerosols [1, 2]. The concepts that play a major role in this kind of studies are the Hurst coefficient and lacunarity.

A. Fractals and Hurst coefficient

Falconer [3] offered a descriptive definition of a fractal: "A set F is fractal if it features the following properties: a) F has a fine structure, say, detail over arbitrarily small scales, b) F is too irregular to be described by traditional geometric language, both locally and globally, c) F features some self-similar forms, either approximate or statistical, d) usually, F's fractal dimension is higher than its topological dimension, e) in most interesting cases, F is defined in a very simple way, maybe, recursively.

Mandelbrot and Van Ness [4] found that the position of a particle with Brownian motion presents scaling properties, which was called ordinary Brownian motion, B(t). Afterwards, they developed the ordinary Brownian motion under a general conception, that means, the fractional Brownian motion, $B_H(t)$, which is currently called fractal Brownian motion, fBm [5]. Mandelbrot and Van Ness [4] proved that if $B_H(t) = 0$ and $H = ½$, then $B_H(t)$ becomes the ordinary Brownian motion. The fractal Brownian motion

(fBm) features a very important property that is known as self-affinity. A real random function, $X_H(0 \leq t < \infty)$, is defined as self-affine with parameter $H \geq 0$ if for any b>0, then $B_H(bt) = b^H B_H(t)$.

As for the fBm, the fractal dimension (D) in the graph described by $B_H(t)$ is $D = 2 - H$, in two dimensions [6]. The fractal parameter (H) is called "Hurst exponent", for it was Hurst who found a scaling relationship that was similar to that of the fBm by means of a new statistical method that was developed by him and that was called "The rescaled range analysis" [7].

B. The Hurst empirical law and the rescaled range (R/S) analysis

The Hurst exponent (H) arose from a classic hydrologic problem. Hurst [8, 9], studying the floods of the river Nile and other problems of water storage, tried to solve the following problem: How to design a dam that never overflows and never dries off? Based on the discharge records of the Lake Albert, Hurst studied the annual discharges as a function of time.

The water volume of the dam depends on the quantity ξ_t coming from the lake, as well as from the regular annual discharge $< \xi >$. If the required storage is such that the dam liberates an annual volume equal to the average quantity of the added water in a given period, then the liberated volume of the dam in one year should be equal to:

$$< \xi > = \frac{1}{h} \sum_{t=1}^{h} \xi_t \, . \qquad (1)$$

The accumulated value of the differences between the entry volume (ξ_t) and the average liberated volume $< \xi >$ is $X(t, h)$:

$$X(t,h) = \sum_{u=1}^{t} [\xi_u - < \xi >] \, . \qquad (2)$$

The range R is defined as the difference between the maximum and minimum values of the accumulated X: where "h" is the considered period and "t" is an integer time value.

$$R(h) = \max_{1 \leq t \leq h} X(t,h) - \min_{1 \leq t \leq h} X(t,h) \, . \qquad (3)$$

Hurst compared the ranges observed for different phenomena such as river discharges, sediments and tree rings. He used the non-dimensional R/S ratio, calling it the rescaled range, where "S" is the standard deviation, obtaining the following general relation [7]:

For diverse time series originated from prospecting geophysical properties, Hurst observed the empirical rule, where he established that the rescaled range grew with time as [7]:

$$S(h) = \left(\frac{1}{h} \sum_{t=1}^{h} \left(\xi_t - < \xi > \right)^2 \right)^{1/2} , \qquad (4)$$

$$R(h) / S(h) = (h/2)^H , \qquad (5)$$

where for the H values that satisfy $0.5 < H < 1$, there is a persistent behavior (that is to say, the increase or decrease of the locally observed curve tends to continue), while $0 < H < 0.5$ implies an anti-persistent behavior (there are no clear tendencies for longer increasing or decreasing intervals) [10].

In the present work, the Hurst coefficients were obtained using the software BENOIT® [11].

C. Lacunarity

The lacunarity concept was proposed as a quantitative measure of the gap-size distribution on a texture [12, 13] and [14]. Lacunarity describes the degree of translation invariance of a point set and becomes a complementary parameter to the fractal dimension, which characterizes the scaling of a measure of points in a domain with the size of the domain [15]. Frequently, objects with equal fractal dimension have visibly different textures. For instance, deterministic Cantor and random Cantor sets have both the same fractal dimension of 0.6309, but the gap size distribution is remarkably different [16, 17].

As for high lacunarity values, they imply the presence of wider gaps; and low lacunarity values refer to a more uniform distribution of gaps of similar size. According to the aforementioned, the presence of an almost uniform distribution is associated with low lacunarity; on the other hand, the presence of points clustered within a single zone is connected with high lacunarity.

Different algorithms have been proposed to quantify lacunarity [18, 19, 20] and [21]. For instance, by using the lacunarity algorithm developed by Allain and Cloitre [21], known as the "gliding box" method, where a box of length r is placed at the origin of one set, the number of occupied sites within the box (box mass equal to s) can be determined. The box is moved one space along the set and the box mass is again counted. This process is repeated over the entire set. The first and second moments are now determined [22]:

$< s(r) >$ is the average and σ^2 is the variance of the occupied site numbers. Therefore [22, 23, 24] lacunarity becomes.

If the distribution is uniform, the variance equals zero and the lacunarity is 1. The lacunarity can be seen as a non-dimensional representation of the ratio (variance)/(mean)^2, and is related to the width of the histogram of the point-density distribution for the given pattern [22, 23].

$$M^{(1)}(r) = \left\langle s(r) \right\rangle . \qquad (6)$$

The plots of $\log_{10}$(lacunarity) vs $\log_{10}$(r) for distributions, appear. From the regular changes of lacunarity with box size several observations can be made:

(1) Non clustered sets have higher lacunarity than dense sets, for the same box sizes;

(2) Bigger boxes tend to be more translation-invariant (the second moment diminishes with the growing box, with

respect to the first moment). Thus, the same set will have lower lacunarities as box size increases [24];

(3) For certain r and fraction p of occupied sites, higher lacunarity will mean higher data clustering [24].

It is observed that for a bigger box size, the deviations approach zero. The lacunarity of the random set gives a concave curve. For randomly distributed clusters, the lacunarity can be used for scale analysis. The curve is almost constant up to crossover point where the tendency changes. In the present work, the Hurst coefficient and lacunarity were used to study experimental atmospheric data.

II. EXPERIMENTAL WORK

Atmospheric sub-micron particle concentrations were measured in the particle size interval ranging from 15.7 to 764nm by means of a Scanning Mobility Particle Sizer [SMPS] (TSI, model 3936), during the MILAGRO field campaign, from March 24 to April 24, 2006, at the Jasso Station, which belongs to the "Compañía de Luz y Fuerza del Centro" (near the "Miguel Hidalgo" refinery in the Tula region), and is approximately located at 60km northwest from Mexico City.

In order to describe the behaviour of aerosols in the region mentioned above, a 24-hour-measurement run was performed by the SMPS; the measurements were taken at ten-minute intervals. The bulk data collected during the different campaign days were analyzed in order to select the campaign days with complete data sets. The selected days to be studied in this work were: March 31, April 1, 4, 6, 7, 8, 9, 10, 11, 13, 15, 17, 18, 19, 20 and 21.

$$M^{(2)}(r) = \sigma^2(r) + \langle s(r) \rangle^2, \tag{7}$$

$$L(r) = \frac{\sigma^2(r)}{\langle s(r) \rangle^2} + 1. \tag{8}$$

The fractal analysis (Hurst coefficient) of the experimental data for the campaign days stated above was carried out by using Eq. (5) through the BENOIT® software. The lacunarity results were obtained by using Eq. (8), which was previously deduced.

III. RESULTS AND DISCUSSION

A. Experimental

Table I shows the maximum local concentration for each selected campaign day, the hour of the day and the corresponding particle diameter. Fig. 1 (a, b, c, d) shows the concentration of particles as a function of time for the campaign days stated above; and Fig. 2 (a, b, c, d) depicts the concentration of particles as a function of diameter for the stated campaign days.

From the maximum concentration values shown in Table I, it can be seen that the first three days were the ones with the highest particle concentrations (more than 2.5 x 10^5 particle/cm^3), while the rest of the days were below 1.1 x 10^5 particle/cm^3. It can also be noted that March 31 was the most contaminated day, whereas April 17 was the cleanest of all. The presence of the three highest concentrations could be explained by some extra activities at the refinery, which took place during these three days, and the corresponding pollution plume was driven from the refinery to the monitoring site because the wind direction coincided with the location of both (30° to the North) at these hours of the day. In addition, the low wind speed (2.5m/s) prevented the efficient dispersion of the particles.

TABLE I. Maximum local concentration, hour of the day and the corresponding particle diameter.

Day/ Month 2006	Local max conc [p/cm^3]	Hour of the day	Particle Diam [nm]
March 31	317753	12:55	38.5
April 1	269637	12:30	15.7
April 4	268426	10:30	24.1
April 6	24143	00:30	16.8
April 7	79980	14:50	21.7
April 8	51005	19:20	76.4
April 9	108446	11:10	35.9
April 10	80035	11:10	21.7
April 11	109855	09:50	46.1
April 13	90024	12:20	15.7
April 15	37681	12:50	18.8
April 17	20875	18:30	37.2
April 18	34770	14:30	15.7
April 19	82198	14:10	16.3
April 20	36368	15:20	41.4
April 21	85447	11:10	21.7

By analyzing Fig. 1, it can be seen that each campaign day exhibited the highest particle concentrations between 8:00 and 17:00h, which were likely emitted by vehicles and industries. In addition, low particle concentrations were measured from 01 to 07h, and also from 18:00 to 23:00h. Only some peaks can be observed between 19:00 and 20:00h, which could be due to pollution coming exclusively from vehicles.

As for particle size, Table I also shows the corresponding particle diameter for each local maximum particle concentration, and it can be observed that the corresponding values were different for each campaign day. The highest particle diameter occurred on April 8 (76.4nm) and the lowest diameters occurred on April 1, 13 and 18 (15.7nm). In the present study, a relationship between the highest local concentration and the particle diameter could be found due to the fact that all possible diameters were included in the concentration analyses. The particle diameter column in Table I refers to both the diameter that contributed the most to the particle concentrations and the prevailing diameters that were observed on each sampling day along the campaign.

Fig. 2 depicts the evolution of the particle diameter for the different concentrations occurring throughout each campaign day; and it can be noticed that each particle size distribution spans over all particle diameters. As for the origin of these particles, it is possible that aerosols with the lowest diameters correspond to fresh emissions, and those with diameters around 50 and 76.4 nm correspond to particles resulting from condensation, coalescence and accumulation processes, among others; and from chemical and photochemical reactions. Such atmospheric processes led to a high variability of the evolution of the particle sizes and the corresponding formation and growth of secondary particles.

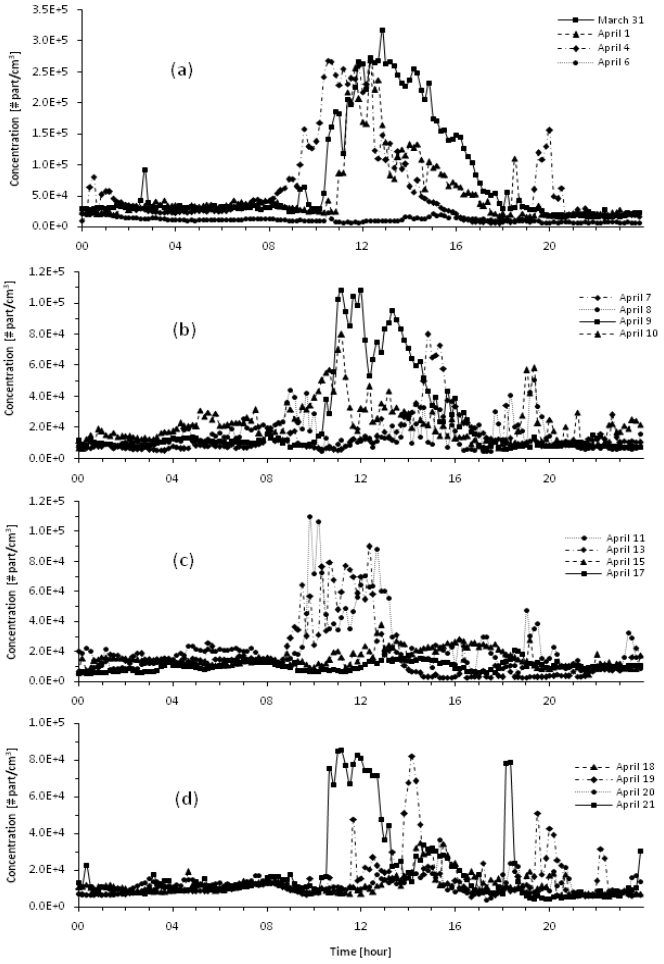

FIGURE 1. Particle concentrations for every hour of the selected monitoring campaign days. The scales of the "y" axes were adjusted to emphasize the corresponding particle concentrations.

With regard to April 9, there were important contributions by sub-micron particle discharges, where both the Power Plant and the Refinery were responsible. In addition, the particle mean diameters were located between 15.7–50nm, which are similar to those found in Light Duty Vehicle tail-pipe exhaust gases.

According to the study of ultrafine particles performed by Dahl *et al*. [25], carbon filling materials (soot agglomerates) and softening fillers (mineral oils) could also be considered as particle sources in this work.

B. Fractal Analysis

As it was mentioned above, in order to perform the fractal analysis of the atmospheric experimental data, the Hurst coefficient and lacunarity were calculated. Table II shows the H and L values concerning the total concentrations, and the concomitant particle formation processes (nucleation, Aitken and accumulation) for each campaign day. By analyzing this table, it can be seen that the Hurst coefficients (H) changed during all the campaign days, whereas the lacunarity values (L) present local maxima and minima.

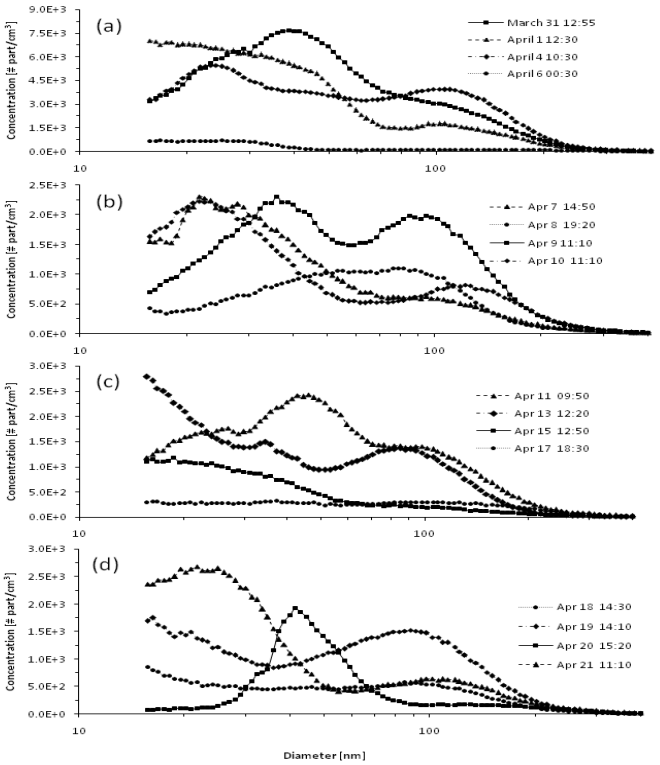

FIGURE 2. Concentration of particles as a function of diameter.

As for the total *H* values, it is observed that the lowest and highest values (0.173 and 0,474) occurred on April 15 and 18, respectively. These results indicate that the aforesaid days were the most and less "dynamic" ones with respect to the variation in the intensity of the atmospheric emissions, because low and high *H* values represent rough and smooth traces, respectively, in a plot. The aforementioned can be graphically seen for all the monitoring days in Fig. 1.

As for total lacunarity, the lowest and highest L values (1.095 and 2.294) occurred on April 17 and 9, respectively. These results indicate that April 17 and 9 were the least and most lacunar days, respectively. The aforesaid means that these days were the ones that displayed the lowest and highest particle concentration distributions (lagoons) throughout time. This fact is also reflected in Fig. 1, where

these "lagoons" can be seen for all the campaign days. From the aforementioned, *H* can be associated with the intensity of the emissions, that is to say that the irregularity of the trace, synthesized by the *H* values, changes depending on the concentration of the different types of particles incorporated into the atmosphere throughout the day.

TABLE II. Hurst coefficient and lacunarity calculated from the nucleation, Aitken and accumulation particle distributions.

Campaign day	Total Conc.		Nucleation		Aitken		Accumulation	
2006	H_{total}	L_{total}	H_N	L_N	H_A	L_A	H_{acc}	L_{acc}
2006-03-31	0.419	2.128	0.417	3.756	0.42	2.342	0.308	1.291
2006-04-01	0.348	1.992	0.334	5.37	0.327	2.148	0.346	1.16
2006-04-04	0.437	2.226	0.284	2.846	0.388	2.33	0.526	2.061
2006-04-06	0.433	1.117	0.336	3.214	0.351	1.186	0.466	1.224
2006-04-07	0.229	1.797	0.152	4.167	0.198	2.21	0.257	1.106
2006-04-08	0.178	1.377	0.134	2.756	0.19	1.563	0.266	1.264
2006-04-09	0.405	2.294	0.233	4.014	0.375	2.578	0.416	1.723
2006-04-10	0.269	1.316	0.279	3.702	0.205	1.439	0.278	1.229
2006-04-11	0.274	1.664	0.294	3.422	0.265	1.942	0.482	1.411
2006-04-13	0.201	2.116	0.244	5.287	0.191	2.387	0.33	1.846
2006-04-15	0.173	1.14	0.207	2.334	0.165	1.21	0.398	1.167
2006-04-17	0.374	1.095	0.621	2.609	0.342	1.14	0.398	1.098
2006-04-18	0.474	1.22	0.211	2.657	0.495	1.399	0.367	1.105
2006-04-19	0.282	1.747	0.263	5.815	0.251	2.107	0.298	1.168
2006-04-20	0.447	1.14	0.372	2.428	0.441	1.373	0.404	1.08
2006-04-21	0.348	2.109	0.482	5.096	0.268	2.323	0.297	1.342

As for particle sizes, the L values indicate the formation of lagoons in the concentration distributions, which gives the idea of how the most important groups were separated according to the different particle diameters (Fig. 2).

By taking into account the particle size intervals associated with the different particle formation processes (nucleation, Aitken and accumulation), the corresponding H and L values were also calculated for all the monitoring days, Table II.

In order to offer a global discussion of the results concerning this section, some monitoring days were selected: March 31, and April 9, 17 and 21. The information of these days is depicted in Fig. 3, where the total, nucleation (10-20nm), Aitken (20-100nm) and accumulation (100-420nm) H and L values are included. From this figure, it can be seen that the H values for the selected days, do not show a pattern connected with the particle formation processes; on the other hand, it can be observed that the high, intermediate and low L values for each selected day represent the nucleation, Aitken and accumulation processes, respectively.

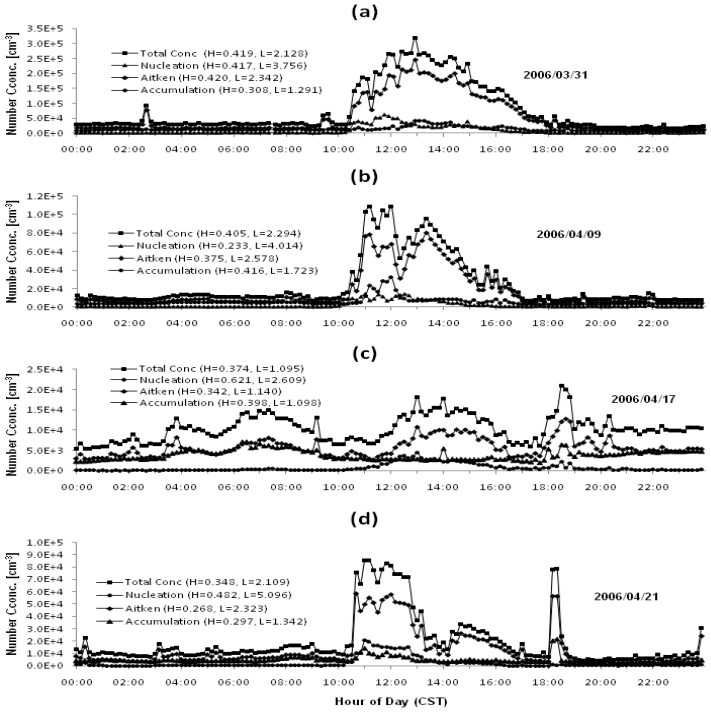

FIGURE 3. Temporal variation of size-fractionated particle number concentration as compared with the total concentration shown in Fig. 1.

As for the different particle formation modes, nucleation presents the highest lacunarity for every day along the campaign, and is the process that separates the most from the global process. This could mean that the ultrafine particles (UFP), with diameters between 10 and 20nm, are incorporated randomly into the atmosphere throughout the day with variable concentrations (Fig. 4).

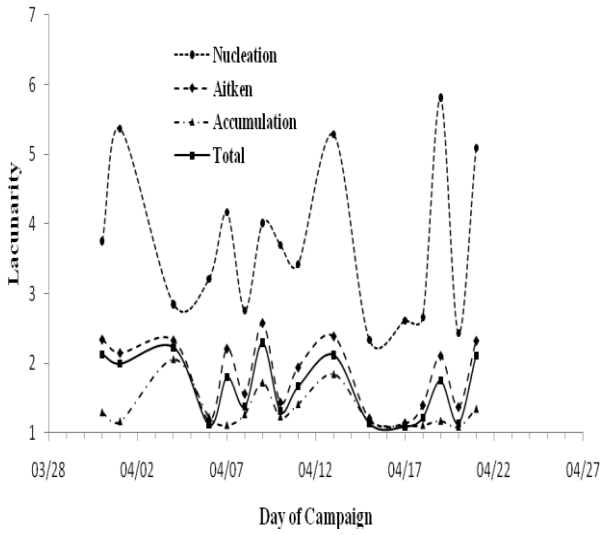

FIGURE 4. Lacunarity for the total concentration, nucleation (N), Aitken (A) and accumulation (acc) modes for the selected campaign days.

On the other hand, the lacunarity plot concerning the Aitken particles, follows the pattern of the total concentration lacunarity curve (correlation coefficient=0.98). This is due to the fact that the Aitken particles (20-100nm) are the main sources of the total concentration and could be considered like the "genetic signature" of the aforesaid concentration. In a different way from the previous cases, the lacunarity curve that depicts the accumulation particles is the lowest, which means a uniform distribution of the particle concentrations in the diameter interval 100-420nm.

These relatively big particles are incorporated into the atmosphere in a uniform way along the day (Fig. 4). By taking into account the last analysis, it can be said that lacunarity can be used to characterize the atmospheric particle formation processes: nucleation, Aitken and accumulation, Fig.4.

With respect to the Hurst coefficient values, the concentration curve associated with the Aitken mode follows the pattern of the total concentration; the roughness of the trace is practically the same (correlation coefficient = 0.96), having similar *H* values (Fig. 5).

IV. CONCLUSIONS

The study of atmospheric particles is of fundamental importance because it enables the researchers to establish many important features concerning this subject matter. Firstly, it characterizes the particles present in the study area by identifying their different sizes. Secondly, it measures the concentration of the particles as a function of time, and reveals the evolution of the particle size distributions, which also helps identify the corresponding particle formation processes. Thirdly, the particle sources i.e. natural or anthropogenic can be identified by analyzing the evolution of the particle size distributions. As an additional contribution of the method, it can be mentioned that it helps evaluate the dispersion of contaminants by quantifying the behavior of the particle distributions throughout time.

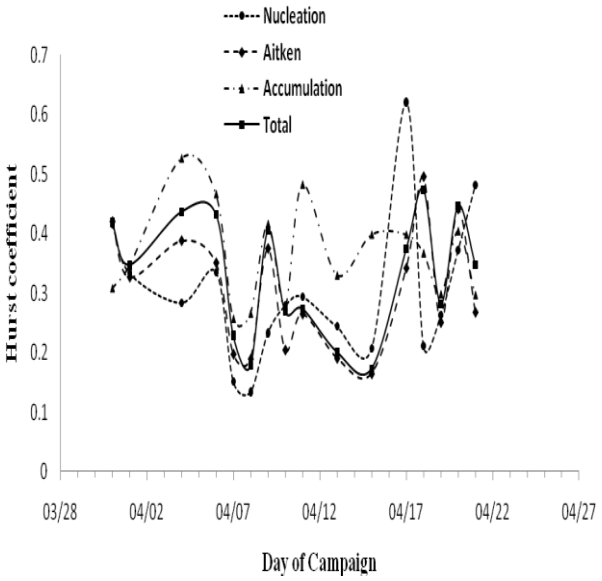

FIGURE 5. The Hurst coefficient for the total concentration, nucleation (N), Aitken (A) and accumulation (acc) modes.

In the present work, besides performing a typical atmospheric particle study, the fractal theory, through the Hurst coefficient and lacunarity concepts, was applied in order to propose a different approach in the study of atmospheric experimental data. The obtained results show that the Hurst coefficient and lacunarity can be useful tools for identifying important changes concerning the particle concentrations (roughness) and size distributions (lagoons), respectively, which occur as a result of dynamic factors such as traffic density, industrial activity and atmospheric conditions (pressure, temperature, humidity, convective currents etc.).

The fractal analysis showed that the *H* values concerning the total concentrations and particle formation processes varied remarkably, showing the random feature of the external emission sources associated with this variable.

By analyzing the lacunarity for the different particle formation processes, it was found that for the different campaign days, the highest, intermediate and lowest values represented the nucleation, Aitken and accumulation processes, respectively; being Aitken the prevalent process in all the analyzed days. As for the Hurst coefficients, it was found that values concerning the total concentration and

Aitken were practically the same. From the aforesaid it can be said that the Aitken process prevailed in the experimental data (lacunarity) and the intensity of this process (Hurst coefficient) was a scale factor of the total concentration. Thus, the main source of the atmospheric particles could be associated with the industrial activity of the region.

Accordingly, it can be said that the fractal analysis is a useful tool to establish intensity fluctuations and distributions of the particle formation processes.

ACKNOWLEDGMENTS

Thanks are due to the "Laboratorio de Caracterización Espectroscópica de Gases y Estudios Ambientales" at the Instituto Mexicano del Petróleo; especially to the areas of "Caracterización y Evaluación de Catalizadores Ambientales and Partículas y Óptica Atmosférica". The authors also acknowledge Sergio Vega for his useful comments to the present work. The anonymous referee's observations were of great value for improving the final version of the manuscript.

REFERENCES

[1] Sosa, G., *Modelación de especies fotoquímicas y partículas suspendidas de la ZMVM*, Doctoral Thesis, CINVESTAV-IPN, México (2002).

[2] Guzmán, R., Sosa, G., Toribio, A., *Efecto del Hollín en la Formación de Nubes*, Molina Center for Energy and the Environment (2002). Available on-line at: <http://mce2.org/newsletter/nwsltr_2/espaniol/Newsletter%202_espanol_small.pdf>, accessed 07.06.10.

[3] Falconer, K., *Fractal Geometry, Mathematical Foundations and Applications*, (Wiley, Chichester, UK, 1990).

[4] Mandelbrot, B. B., Van Ness, J. W., *Fractional Brownian Motions, Fractional Noises and Applications*, SIAM Review **10**, 422-437 (1968).

[5] Li, J. M., Lü, L., Lai, M. O., Ralph, B., *Image-based fractal description of microstructures*, (Kluwer Academic Publishers, Boston, USA, 2003).

[6] Voss, R. F., *Random fractals: Self-affinity in noise, music, mountains, and clouds*, Physica D **38**, 362-371 (1989).

[7] Feder, J., *Fractals*, (Plenum Press, New York, 1988).

[8] Hurst, H. E., *Long-term storage capacity of reservoirs*, Transactions of the American Society of Civil Engineers **116**, 770-880 (1951).

[9] Hurst, H. E., *Methods of using long-term storage in reservoirs*, Proceedings-Institution of Civil Engineers, Part I, **5**, 519-590 (1956).

[10] Mandelbrot, B. B., *Gaussian Self-Affinity and Fractals: Globality, the Earth, 1/f Noise, and R/S*, (Springer-Verlag, New York, 2002).

[11] *BENOIT® Software, Benoit Fractal Analysis Systems*, Version 1.3., (Trusoft International Inc., St. Petersburg, FL 33704 USA, 2009).

[12] Mandelbrot, B. B., *The Fractal Geometry of Nature*, (W. H. Freeman and Co., New York, 1983).

[13] Korvin, G., *Fractals Models in the Earth Sciences*, (Elsevier, Amsterdam, 1992).

[14] Korvin, G., *Tutorial on Lacunarity*, (Unpublished Lecture Note, UNAM, Mexico City, 2002).

[15] Tolle, C. R., McJunkin, T. R., Rohrbaugh, D. T., LaViolette, R. A., *Lacunarity definition for ramified data sets based on optimal cover*, Physica D **179**, 129-152 (2003).

[16] Turcotte, D. L., *Fractal and Chaos in Geology and Geophysics*, 2nd Ed. (Cambridge University Press, New York, USA, 1997).

[17] Turcotte, D. L., *Fractals in petrology*, Lithos **65**, 261-271 (2002).

[18] Gefen, Y., Meir, Y., Mandelbrot, B. B., Aharony, A., *Geometric implementation of hypercubic lattices with noninteger dimensionality by use of low lacunarity fractal lattices*, Physical Review Letters **50**, 145-148 (1983).

[19] Gefen, Y., Aharony, A., and Alexander, S., *Anomalous Diffusion on Percolating Clusters*, Physical Review Letters **50**, 77-80 (1983).

[20] Lin, B., Yang, Z. R., *A suggested lacunarity expression for Sierpinki carpets*, Journal of Physics A **19**, L49-52 (1986).

[21] Allain, C., Cloitre, M., *Characterizing the lacunarity of random and deterministic fractal sets*, Physical Review A **44**, 3552-3558 (1991).

[22] Plotnick, R. E., Gardner, R. H., Hargrove, W. W., Prestegaard, K., Perlmutter, M., *Lacunarity analysis: A general technique for the analysis of spatial patterns*, Physical Review E **53**, 5461-5468 (1996).

[23] Pendleton, D. E., Dathe, A., Baveye, P., *Influence of image resolution and evaluation algorithm on estimates of the lacunarity of porous media*, Physical Review E **72**, 1-9 (2005).

[24] Gao, Z., and Yang, Z. R., *Dynamic scaling behavior of the Ziff-Gulari-Barshad model on regular fractal lattices: The influence of lacunarity*, Physical Review E **59**, 2795-2800 (1999).

[25] Dahl, A., Gharibi, A., Swietlicki, E., Gudmundsson, A., Bohgard, M., Ljungman, A., Blomqvist, G., Gustafsson, M., *Traffic-generated emissions of ultrafine particles from pavement–tire interface*, Atmospheric Environment **40**, 1314-1323 (2006).